

An Approach for Enhancement of MR Images of Brain Tumor

Hare Krishna Mishra*, Manpreet Kaur

Department of Electrical and Instrumentation Engineering, Sant Longowal Institute of Engineering and Technology,
Longowal, Sangrur 148106, Punjab, India

Corresponding Author Email: hare_pei1508@sliet.ac.in



<https://doi.org/10.18280/ts.390405>

ABSTRACT

Received: 7 June 2022

Accepted: 2 August 2022

Keywords:

magnetic resonance images, Bi-Histogram equalization with adaptive sigmoid function, elephant herding optimization, comprehensive learning, Friedman's mean rank test

Magnetic Resonance Imaging plays an important role in diagnosing the brain tumor accurately, but it requires the approach to enhance the magnetic resonance images to assist physicians in brain tumor detection and making the treatment plan precisely to reduce the mortality rate. Therefore, in this proposed work, a comprehensive learning-based elephant herding optimization technique has been introduced to select the optimal value of smoothness factor in Bi-Histogram Equalization with Adaptive Sigmoid Function that enhances the visual quality as well as the appearance of the suspicious regions in magnetic resonance images. Further, the enhancement performance has been evaluated by the enhancement quality metrics. The metrics used include mean square error, peak signal to noise ratio, mean absolute error, structural similarity index metric, feature similarity index metric, Riesz transformed based feature similarity index metric, spectral residual-based similarity index metric, and absolute mean brightness error. The outcomes of this proposed work have a remarkable impact on enhancing magnetic resonance images and providing visual assistance for diagnosing brain tumors. The performance of the evaluation metrics is verified with Friedman's mean rank test, which strongly indicates a statistical difference between the proposed method and state-of-the-art methods.

1. INTRODUCTION

A brain tumor is a cell growth that is uncontrolled in any brain area [1]. A total of 400000 cases of brain tumors are diagnosed globally every year, of which 120000 patients become cancerous due to late diagnosis [2]. As per the GLOBOCAN 2020 report, 308102 new cancerous brain tumor (1.6% of total cancerous tumor) cases were added in 2020, and 251329 lost their life (2.5% overall mortality rate due to cancerous tumor) worldwide [3]. According to the central nervous system of India, around 0.005% to 0.01% of the population is diagnosed with brain tumors, of which 2% have cancerous brain tumors [4]. According to the American Brain Tumor Association and the World Health Organization (WHO), the brain tumor grading system employs a range from one to four grades for designating tumors as malignant or non-cancerous [5]. According to this scale, grades I and II fall under non-cancerous (Benign) tumors and are slow growth rate tumors. Therefore, patients with grade II tumors need proper monitoring and regular observation to cure well on time before these become grade III or malignant. Grades III and IV are categorized as malignant tumors and are high-grade tumors with high growth rates [6]. The above grading plays an essential role in the survival of brain tumor patients that depends on the accurate detection of brain tumors. Medical imaging techniques are adopted these days to diagnose brain tumors. Non-invasive diagnosis methods in medical imaging [7], Computed Tomography (CT) [8], and Magnetic Resonance Imaging (MRI) are widely used in the present scenario. MRI gives more valuable information than CT for brain tumor detection and provides a tumor progress model

during treatment [9]. MRI techniques of image modalities of brain tumors help experts with early diagnosis and treatment. The MR images may contain some noise, and this may affect the accurate diagnosis of brain tumors. Thus it requires enhancing the image quality to increase the detection accuracy of brain tumors.

In this paper, an approach for enhancing the MR images is proposed. The Comprehensive Learning-based Elephant Herding Optimization technique has been proposed to optimize the smoothness factor of Bi-Histogram Equalization with Adaptive Sigmoid Function (BEASF), which gives better results in terms of visual inspection as well as parametric evaluation metrics. The enhanced images show better feature variance without distracting the structural similarity index metrics of brain tumor MR images.

The rest of the paper is organized as follows. The existing work in the field of MR image enhancement is presented in Section 2. the material and proposed methodology are described in Section 3. Section 4 contains information regarding the database used. The output findings and the Friedman rank test is presented in Section 5 to examine the ranking of the proposed methodology. Finally, Section 6 summaries the proposed approach and its future scope.

2. LITERATURE REVIEW

MRI is the most extensively utilized imaging technology for detecting tumor cells. Different MRI techniques like T1-weighted, T2-Weighted, and FLAIR are commonly used. During the imaging process, some noise also enters these

images, which affects the contrast of the image. So it becomes difficult to detect the region that has a tumor. The work of researchers who have adopted various strategies to enhance MR images is covered in this section.

Wood and Runge proposed denoising using a sigma filter [10]. Xue et al. [11] proposed a method for denoising using wavelet thresholding. Christensen [12] proposed a technique for smoothening the histogram, boxcar filtering, that was helpful for image normalization. Weisfeld and Warfield [13] used KullbackLeibler Divergence to normalize the intensities within an image for improved segmentation. Joshi et al. [14] presented a skull stripping procedure to improve the region of interest, allowing medical specialists to diagnose patients more accurately. Liu et al. [15] proposed an algorithm where they first applied clustering. After that, they used histogram normalization to increase the contrast between brain metastases and surrounding tissues. Rajeesh et al. [16] proposed a wave atom shrinkage filter for denoising and enhancement. Khademi et al. [17] proposed an edge-preserving smoothing filter to remove the unused parts of MR images, enhance the region of interest, and increase noise attenuation. Rallabandi and Roy [18] proposed a stochastic resonator algorithm for denoising the images and gave an enhancement factor. Bandyopadhyay [19] presented histogram equalization with median filter, unsharp masking, thresholding, and mean filter for noise removing before segmentation by region growing. George and Karnan [20] proposed a center-weighted median filter for denoising and compared it with the median and weighted median filter. Birla and Shantaiya [21] employed a combination of blind convolution techniques, median filter, and Wiener filter. Sharma and Meghrajani [22] suggested a method for enhancing the contrast of low-intensity greyscale MR images with histogram equalization. Benson and Lajish [23] proposed an algorithm for skull stripping of the brain via mathematical morphology. Chen et al. [24] proposed a method using hierarchical correlation histogram analysis to automatically modify image contrast in three primary atrophic cell regions of MR images of Parkinson's disease patients. Natteshan and Jothi [25] suggested a method in which the image was first denoised with a Wiener filter. Then contrast was enhanced with Contrast Limited Adaptive Histogram Equalization (CLAHE). Integrating intuitionistic fuzzy filtering with fusion operators was introduced by Deng et al. [26] to improve the normal and abnormal structure areas. Kaur and Rani [27] recommended CLAHE after comparing their results with the other histogram equalization methods for image enhancement. Viswanath [28] proposed a combination of color enhancement by scaling and power-law transformations. They adjusted local background illumination, and then they applied power law transformation. Min and Kyu [29] introduced median and Wiener filters for denoising. Subramani and Veluchamy [30] suggested a Brightness Preserving Adaptive Fuzzy Histogram Equalization. Mzoughi et al. [31] recommended an adaptive histogram equalization. Singh et al. [32] proposed a technique where they used a Wiener filter for denoising. Then local transformation-based histogram equalization was used to enhance the image quality. Bhateja et al. [33] proposed a human visual system-based particle swarm optimization technique. Acharya and Kumar [34] introduced particle swarm optimized texture-based histogram. Vidyasaraswathi and Hanumantharaju [35] presented a Gray Wolf Optimization Histogram Equalization-based mean intensity replacement approach. Ullah et al. [36] presented a mathematical

morphological algorithm and histogram equalization for contrast enhancement. Sabitha et al. [37] developed a binary flower pollination technique and binary Particle Swarm Optimization to enhance brain tumor MR images.

It has been observed from the literature that researchers have mostly used histogram equalization methods. The parameter optimization of a histogram-based method results in a better performance. It has been observed from the literature that metaheuristic techniques are used widely for the enhancement of MR images of brain tumors. There is still a need to improve the augmentation of brain tumor areas in MR images so that abnormalities are appropriately recognized and categorized for improved brain tumor diagnosis.

3. MATERIAL AND METHOD

An approach for enhancing MR images has been described in this paper. Compared to other techniques, the output of Bi-Histogram Equalization with Adaptive Sigmoid Function (BEASF) is superior without sacrificing image information [38]. But the problem with BEASF is the selection of an optimal value of the smoothening factor. So an improved metaheuristic technique is required for this purpose. A comprehensive learning strategy is employed to improve the performance of EHO, and this improved EHO is used for optimizing the value of smoothening factor in the BEASF.

3.1 Bi-Histogram equalization with adaptive sigmoid function

BEASF gives more visual quality than original images and ignores brightness preservation. Its qualitative parameters indicate that it preserves brightness [39]. BEASF, contains three steps i.e. histogram splitting, creation of sigmoid function, and mapping [40].

3.1.1 Histogram splitting

The original image (I_1) with the size $M \times N$ has the possible intensity levels (\mathcal{E}). The mean intensity of the image is:

$$\text{Mean Intensity } (m) = \frac{\sum_{i=0}^{M-1} \sum_{j=0}^{N-1} I_1(i, j)}{M \times N} \quad (1)$$

Using the mean intensity as a splitting point, the original image histogram H is separated into two sub-histograms, H_1 and H_2 , $H = H_1 \cup H_2$, where $H_1 = \{h_0, h_1, \dots, h_m\}$ and $H_2 = \{h_{m+1}, h_{m+2}, \dots, h_{\mathcal{E}-1}\}$.

The value of the probability density function of two sub histograms is evaluated after splitting. The probability density function is:

$$p_1(k) = \frac{H_1(k)}{\sum_{n=0}^m H_1(n)} \quad (2)$$

$$p_2(k) = \frac{H_2(k)}{\sum_{n=m+1}^{\mathcal{E}-1} H_2(n)} \quad (3)$$

where, $k \in \{0, 1, 2 \dots \mathcal{E} - 1\}$ is an intensity level.

The cumulative distribution functions for H_1 and H_2 are:

$$c_1(k) = \sum_{n=0}^k p_1(n) \quad (4)$$

$$c_2(k) = \sum_{n=m+1}^k p_2(n) \quad (5)$$

Then μ_1 and μ_2 are the medians of sub histogram H_1 and H_2 can be found when the following conditions are satisfied.

$$c_1(\mu_1) = 0.5 \text{ and } c_2(\mu_2) = 0.5.$$

3.1.2 Sigmoid function creation

In this process, two parametric nonlinear sigmoid functions (Eq. (8) and (9)) are created by taking the origins of the sigmoid functions at the medians defined in sub-histograms. The value of k is normalized using the following Eq. (6) and (7):

$$z_1(k) = \frac{5(k-\mu_1)}{m}, k \leq m \quad (6)$$

$$z_2(k) = \frac{5(k-\mu_2)}{\ell-1-m}, k > m \quad (7)$$

Here ' $z_1(k)$ ' and ' $z_2(k)$ ' are the input values used for the calculation of the sigmoid function, ' k ' is the intensity level, ' m ' is the mean intensity, μ_1 and μ_2 are the medians of sub-histogram H_1 and H_2 , ℓ is the possible intensity levels.

$$s_1(k) = \frac{1}{1+e^{-\gamma z_1(k)}}, k \leq m \quad (8)$$

$$s_2(k) = \frac{1}{1+e^{-\gamma z_2(k)}}, k > m \quad (9)$$

Here, $s_1(k)$ and $s_2(k)$ are non-linear parametric sigmoid functions, ' k ' is the intensity level, and γ is the smoothness factor.

After the normalization of the sub histogram, it will fit the desired boundaries of the sigmoid function, $z_1(k), z_2(k) \in [-5,5]$, the convenient range for sigmoid function, the values of smoothening factor across this range will be either 0 or 1.

For the above sigmoid function, the range will be $[0, m]$ and $[m, \ell-1]$. The smoothness factor of the sigmoid function is γ . A smoother sigmoid function is created by a lower value of γ , which affects the value of contrast in the enhanced image.

3.1.3 Mapping

The sigmoid function calculated in the previous steps is utilized for finding the values of histogram equalization and stretching. The formulation of the histogram equalization is as follows:

$$u_1(k) = L_0 + (m - L_0) s_1(k) \quad (10)$$

$$u_2(k) = m + (L_1 - m) s_2(k) \quad (11)$$

L_1 and L_0 are the desirable upper and lower limit of the dynamic range in enhanced images, here $L_0=0$ and $L_1=\ell-1$. After mapping, the histogram stretching has been performed by using the equation below:

$$STF = \begin{cases} L_0 + \alpha_1(u_1(k) - \min(u_1)) & \text{when } k \leq m \\ m + \alpha_2(u_2(k) - \min(u_2)) & \text{when } k > m \end{cases} \quad (12)$$

where, $\alpha_1 = \frac{m-L_0}{\max(u_1)-\min(u_1)}$ and $\alpha_2 = \frac{L_1-m}{\max(u_2)-\min(u_2)}$.

The mappings calculated in this step are applied to every pixel of the input image for image enhancement.

3.2 Elephant herding optimization

The EHO method was introduced by Wang et al. [41]. The process of EHO depends on the herding behavior of elephants. After growing up, the male elephants leave their families to form their self-groups. The elephants are divided into distinct clans and live together under the direction of a matriarch. The two behaviors described above are represented using two operators. The clan updating operator and the separation operator are idealized to construct a simple global optimization approach.

3.2.1 Clan updating operator

When the elephants are moving surrounding the matriarch, the positions of individual elephants in the clan are marked by the matriarch after every movement of individuals. Then the newest position of the elephant is considered as:

$$E_{new,Q_n,k} = E_{Q_n,k} + \delta \times (E_{best,Q_n,k} - E_{Q_n,k}) \times t \quad (13)$$

where, $E_{new,Q_n,k}$ is the elephant's latest position in the clan. $E_{Q_n,k}$ is the k^{th} elephant's old position in the clan Q_n . E_{best,Q_n} is the fittest elephant in clan Q_n , $t \in [0,1]$, is a uniformly distributed random number. $\delta \in [0,1]$ is a factor by which $E_{Q_n,k}$ affected by matriarch Q_n . It is also known as the scaling factor. The fittest elephants in the clan are represented as:

$$E_{new,Q_n,k} = \gamma \times E_{centre,Q_n} \quad (14)$$

$E_{new,Q_n,k}$ is getting the data of all elephants present in the clan. $\gamma \in [0,1]$, factor by which influence of E_{centre,Q_n} on $E_{new,Q_n,k}$ is determined. $E_{centre,Q_n,d}$ is the center of the clan Q_n for the d^{th} dimension and can be obtained by the following equation:

$$E_{centre,Q_n,d} = \frac{1}{\theta_{Q_n}} \times \sum_{k=1}^{\theta_{Q_n}} E_{Q_n,k,d} \quad (15)$$

where, $1 \leq d \leq D$ shows the d^{th} dimension in which D is the total dimension.

3.2.2 Separating operator

When male elephants complete their grown-up stage in the clan, they leave the family group. Enhancement of EHO algorithm searching capability within a condition when for every generation, the separating operator is completed by all individual elephants with worst fitness is described as follows:

$$E_{worst,Q_n} = E_{min} + (E_{max} - E_{min} + 1) \times rand \quad (16)$$

where, E_{worst,Q_n} is, the worst's elephant in the clan, $rand$ represents the stochastic and uniform distribution having range between $[0, 1]$. E_{max} and E_{min} are the individual elephant's upper and lower bound positions.

3.3 Comprehensive learning-based EHO (CLEHO)

The standard EHO has some drawbacks. Due to the updating operator, the exploration is influenced by unreasonable convergence towards the origin and unbalanced exploration [42]. The clan-updating operator may only update clans inside its own [43]. Therefore, comprehensive learning

[44] is introduced in this work to improve the drawbacks of standard EHO. In comprehensive learning, three different learning strategies have been introduced to update the positions of elephants that are described below:

3.3.1 Learning strategy I

For improving the exploration of the algorithm, Eq. (17) is used, and it gives better results. It depends on the worst and best clan individuals of the current clan to enhance the searchability of EHO.

$$E_{new,Q_n,k} = E_{Q_n,k} + (\varphi_1 \times E_{best,Q_n,k} - |E_{Q_n,k}|) - \varphi_2(E_{worst,Q_n,k} - |E_{Q_n,k}|), \quad (17)$$

if $0 \leq T_{switch} \leq 1/3$

φ_1 and φ_2 are the two random numbers, and T_{switch} is switch probability and distributed uniformly between 0 to 1.

3.3.2 Learning strategy II

In this strategy, the mean and best clan individuals are used to update the positions of the current clan individual. It is expressed as:

$$E_{new,Q_n,k} = E_{Q_n,k} + (\varphi_3 \times E_{best,Q_n,k} - |E_{Q_n,k}|) - \varphi_4(\bar{X} - |E_{Q_n,k}|), \quad (18)$$

if $\frac{1}{3} < T_{switch} \leq 2/3$

where, \bar{X} is the mean position of the clan. φ_3 and φ_4 are the two random numbers subjected to normal distribution.

3.3.3 Learning strategy III

This strategy utilizes the position of the worst clan individual and two randomly selected clan individuals to update the position of the current clan individual. This strategy is mathematically modeled as:

$$E_{new,Q_n,k} = E_{Q_n,k} + (\varphi_5 \times E_{best,Q_n,k} - E_{Q_n,k}) - \varphi_6(E_p - E_q), \quad (19)$$

if $\frac{2}{3} < T_{switch} \leq 1$

where, p and q are two integer ranges between one to θ_{Q_n} and not equal to each other, at any instance. φ_5 and φ_6 are the two random numbers between zero and one.

3.4 Proposed methodology

In the proposed work, a Comprehensive Learning-based Elephant Herding Optimization (CLEHO) is proposed to enhance MR images of brain tumors, taking 1577 images from the Figshare [45] data set publicly available. The proposed CLEHO algorithm is used for optimizing the value of the smoothness factor (γ) of the sigmoid function of BEASF. The proposed CLEHO optimizes the smoothness factor by initiating random solutions and further improves them by selecting a learning strategy based on the switching probability (T_{switch}). In this manner, CLEHO gives the best value for the smoothness factor.

4. DATABASE

The dataset used for this work is taken from Figshare [45].

The dataset contains 3064 T₁ contrast-enhanced MR images of brain tumors of 233 patients. The dataset contains three widely classified primary brain tumors glioma, meningioma, and pituitary. The dataset includes 89 patients with glioma with 1436 images, 82 patients with meningioma with 708 images, and 62 patients with pituitary having 930 images. MR images of brain tumors are available in three different positional views of the brain coronal, sagittal, and axial. The images are available as .mat files, including the tumor mask's details, patient ID, and tumor label. For each image, the region of suspicion, cropped manually, is considered for further processing.

5. RESULTS AND DISCUSSION

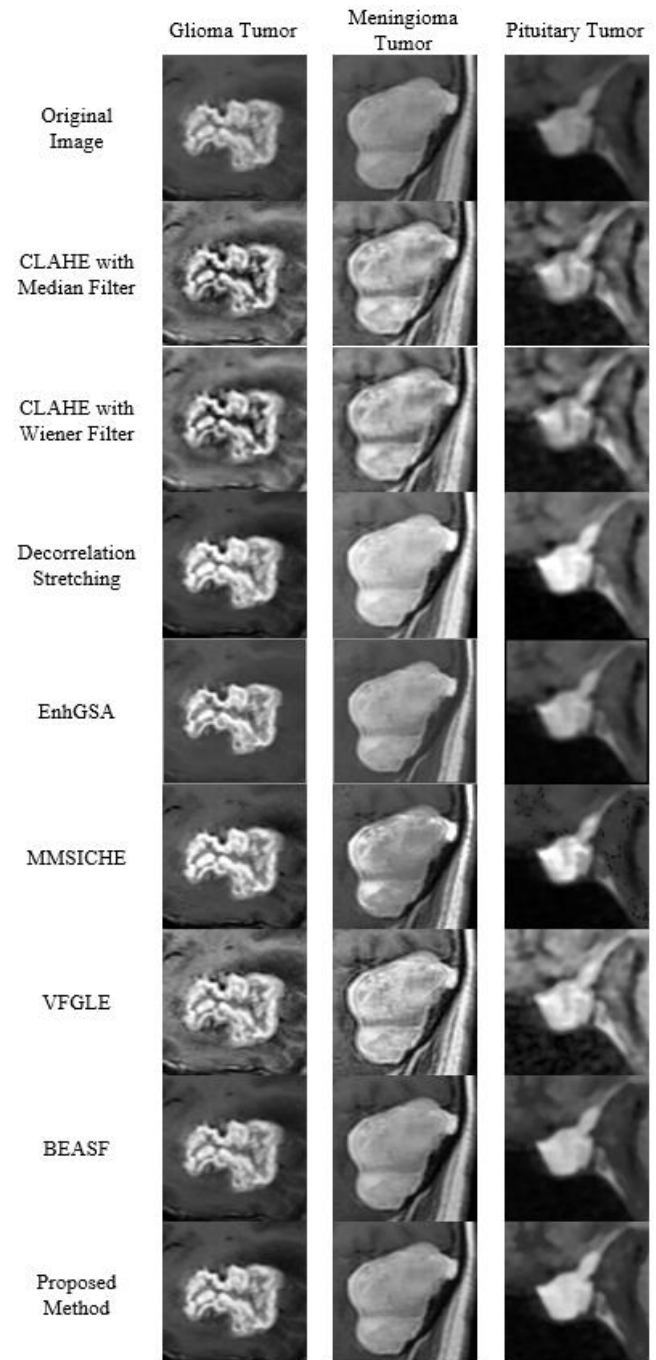


Figure 1. Visual analysis of original and enhanced images

A methodology using Comprehensive Learning-based

Elephant Herding Optimization (CLEHO) is employed to optimize the smoothing factor of BEASF, which is used to enhance the image quality of MR images. For the proposed CLEHO-based approach, the population is 50, and 500 iterations are taken to optimize the value of the smoothness factor (γ) of the Bi-Histogram equalization with adaptive sigmoid function. The experimental results are performed on an Intel I3 7th generation processor system using Windows 10 Pro operating system having 8 GB RAM. The proposed methodology has been implemented in MATLAB2021a.

The proposed methodology has processed glioma, meningioma, and pituitary tumor images. The region of suspicion is extracted by cropping the area of interest, and images collected from the Figshare database have been taken for testing. The performance has been evaluated for direct visual inspection and quantitative analysis of glioma, meningioma, and pituitary tumors.

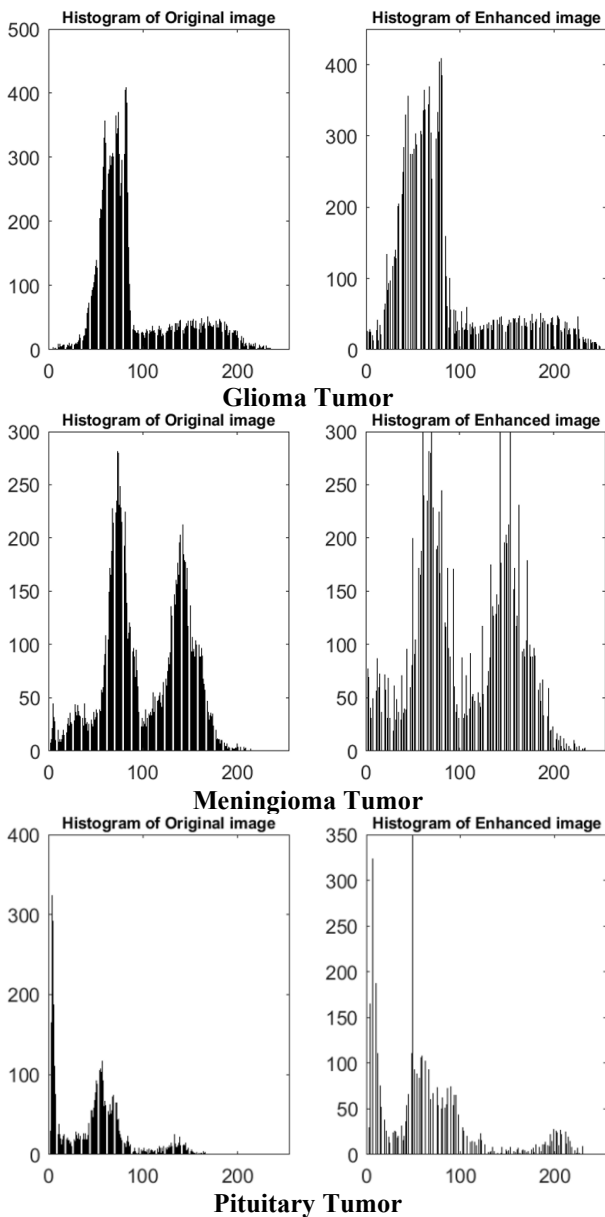


Figure 2. Histogram comparison of original and enhanced images

5.1 Visual inspection

A total of 1577 images are taken for visual inspection in

which it has been seen that the region of interest is enhanced. The histograms showing the number of pixels for each tonal value are plotted. It describes the tonal distribution of an image. The proposed method is compared with CLAHE with Median filter [46], CLAHE with Wiener filter [25], Decorrelation [47], Enhancement Gravitational Search Algorithm (EnhGSA) [48], Median Mean based Sub Image Clipped Histogram Equalization (MMSICHE) [49], Variational based Fusion model for Gray Scale image Enhancement (VFGLE) [50], and Bi-Histogram Equalization with Adaptive Sigmoid Function (BEASF) [40]. The visual comparison of the proposed method with other state-of-the-art methods by taking an image from three different type of tumors, shown in Figure 1.

Figure 1 shows that the proposed technique successfully enhances the MR images of all three tumor types. The enhanced images give a better outcome than the other method without losing their originality. A comparison of histograms for the original and enhanced image is shown in Figure 2.

Through visual inspection, it is observed that the contrast and intensity of the enhanced images are stretched only up to that limit where the enhanced images do not lose their visual properties. The enhanced images (Glioma tumor - 832, Meningioma tumor - 677, pituitary tumor - 1756) shown have not sacrificed any significant image information.

5.2 Quantitative evaluation

Improving the visual quality of a digital image, often known as image enhancement, is a subjective process. The identification of one method that provides a better quality image may vary from person to person. So, metrics to compare the effects of image enhancement algorithms on image quality are required for proper analysis. Mean Square Error (MSE), Peak Signal to Noise Ratio (PSNR), Mean Absolute Error (MAE), Structural Similarity Index Metric (SSIM), Features Similarity Index Metric (FSIM), Riesz transformed based Feature Similarity Index Metric (RFSIM), Spectral Residual base Similarity Index Metric (SRSIM) and Absolute Mean Brightness Error (AMBE) are used for quantitative evaluation of the proposed work. For the quantitative assessment, four images of each type are taken. 901, 796, 1899, and 2300 are of glioma type, while 99, 500, 245, and 281 meningioma type. 1689, 1546, 1332, and 1389 are taken from the pituitary tumor type.

5.2.1 Mean Square Error (MSE)

It is the cumulative squared error between enhanced and original images, and its values are always positive [51]. MSE is calculating the difference between the original and processed images. Mathematically, it is written as:

$$MSE = \frac{1}{M \times N} \sum_{i=0}^{M-1} \sum_{j=0}^{N-1} (I_2(i, j) - I_1(i, j))^2 \quad (20)$$

where, I_2 is the enhanced image of an original image I_1 with dimensions $M \times N$. Table 1 compares the results of MSE when four images of each tumor type are included. It has been observed that the values of MSE for all three types of brain tumors MR images are the lowest for the proposed methodology. In Table 1, the next best MSE value given by BEASF indicates the large performance gap with the proposed method. MMSICHE and EnhGSA are the least performers in Table 1 with regard to the performance of MSE.

Table 1. Mean square error value

Method	Glioma Tumor				Meningioma Tumor				Pituitary Tumor			
	901	796	1899	2300	99	500	245	281	1689	1546	1332	1389
CLAHE with Median Filter	0.0094	0.0246	0.0103	0.0171	0.0218	0.0177	0.0201	0.0142	0.0325	0.0234	0.0132	0.0113
CLAHE with Wiener Filter	0.0086	0.0221	0.0092	0.0147	0.0246	0.0280	0.0265	0.0182	0.0337	0.0266	0.0148	0.0142
Decorrelation Stretching	0.0125	0.0440	0.0185	0.0274	0.0303	0.0238	0.0660	0.0296	0.0770	0.0305	0.0486	0.0134
EnhGSA	1992.2	714.17	1777.6	2702.2	1686.3	1556.4	2213.1	464.77	2432.7	1619.6	1949.5	4399.9
MMSICHE	561.14	850.24	723.68	842.46	587.44	686.54	417.33	581.98	1001.7	864.62	1241.2	376.65
VFGLE	0.0160	0.0771	0.0251	0.0345	0.0302	0.0417	0.0243	0.0298	0.0753	0.0638	0.0673	0.0228
BEASF	0.0022	0.0033	0.0029	0.0040	0.0021	0.0029	0.0022	0.0017	0.0028	0.0028	0.0020	0.0036
Proposed Method	0.00002	0.00003	0.00003	0.00003	0.00002	0.00002	0.00003	0.00003	0.00002	0.00002	0.00003	0.00003

Table 2. Peak signal to noise ratio value

Method	Glioma Tumor				Meningioma Tumor				Pituitary Tumor			
	901	796	1899	2300	99	500	245	281	1689	1546	1332	1389
CLAHE with Median Filter	20.22	16.07	19.86	17.65	16.60	17.51	16.96	18.46	14.86	16.29	18.78	19.43
CLAHE with Wiener Filter	20.63	16.54	20.32	18.32	16.08	15.52	15.76	17.37	14.72	15.74	18.28	18.46
Decorrelation Stretching	19.00	13.56	17.30	15.61	15.18	16.23	11.79	15.28	11.13	15.15	13.12	18.70
EnhGSA	15.13	19.59	15.63	13.81	15.86	16.20	14.68	21.45	14.26	16.03	15.23	11.69
MMSICHE	20.64	18.83	19.53	18.87	20.44	19.76	21.92	20.48	18.12	18.76	17.19	22.37
VFGLE	17.93	11.12	15.99	14.62	15.19	13.79	16.13	15.25	11.22	11.95	11.71	16.41
BEASF	26.56	24.79	25.35	23.95	26.61	25.36	26.38	27.52	25.41	25.49	26.82	24.37
Proposed Method	45.23	45.16	44.29	44.10	45.49	45.35	45.11	45.11	45.90	45.32	44.97	44.82

Table 3. Mean absolute error value

Method	Glioma Tumor				Meningioma Tumor				Pituitary Tumor			
	901	796	1899	2300	99	500	245	281	1689	1546	1332	1389
CLAHE with Median Filter	0.0781	0.1389	0.0810	0.1068	0.1271	0.1048	0.1136	0.0966	0.1526	0.1341	0.0993	0.0881
CLAHE with Wiener Filter	0.0745	0.1316	0.0752	0.1002	0.1332	0.1435	0.1345	0.1091	0.1554	0.1436	0.1061	0.0972
Decorrelation Stretching	0.0984	0.1691	0.1205	0.1332	0.14951	0.1344	0.2198	0.1593	0.2478	0.1298	0.1721	0.0977
EnhGSA	0.0036	1.639	1.105	.0925	3.769	0.0974	0.5637	3.616	0.2630	0.1634	0.0461	0.0231
MMSICHE	3.452	3.487	2.494	5.730	0.8339	0.8113	0.9423	2.2051	0.5177	1.2518	2.5070	0.4661
VFGLE	0.1069	0.2368	0.1283	0.1491	0.1526	0.1777	0.1331	0.1444	0.2413	0.2253	0.2321	0.1340
BEASF	0.0320	0.0422	0.0347	0.0340	0.0407	0.0449	0.0413	0.0344	0.0461	0.0416	0.0402	0.0450
Proposed Method	0.0043	0.0040	0.0048	0.0049	0.0043	0.0043	0.0044	0.0044	0.0041	0.0043	0.0043	0.0045

5.2.2 Peak signal to noise ratio (PSNR)

It is the ratio between the maximum possible power of an image and the power of corrupting noise [52]. It was previously used to determine image reconstruction quality [24], [53]. Mathematically it is expressed as:

$$PSNR = 10 \log_{10} \frac{(2^n - 1)^2}{MSE} \quad (21)$$

where, n is the number of bits in one pixel of the image.

A higher PSNR value and a lower MSE value indicate a superior Signal-to-Noise Ratio (SNR). The proposed approach is compared to the PSNR values of images obtained with seven different methods, and the results of 12 images are given in Table 2.

The proposed method has a higher value of PSNR than other state-of-the-art methods. A large margin between the proposed and next performer (BEASF) is indicated in Table 2. VFGLE performs the worst with a minimum average value of PSNR.

5.2.3 Mean absolute error (MAE)

It is a metric for comparing errors between paired observations that describe the same occurrence. The difference between the average intensity of the original image and that of the enhanced image is the mean absolute error in medical image processing [54]. MAE is calculated as:

$$MAE = \frac{\sum_{i=0}^{M-1} \sum_{j=0}^{N-1} |I_1(i, j) - I_2(i, j)|}{M \times N} \quad (22)$$

where, I_1 is the original image and I_2 is the enhanced image. The lowest value of mean absolute error shows better quality features [55]. The MAE values are very low in the proposed method compared to other state-of-the-art methods (Table 3).

The gaps between the proposed and the next techniques indicate the significance of the proposed work.

5.2.4 Structural similarity index metric (SSIM)

SSIM is a non-cognitive parameter that indicates how image quality deteriorates during image processing. A larger SSIM value is necessary for the more remarkable preservation of contrast, structural content, and brightness. Its maximum value is close to one [56]. Mathematically it is expressed as:

$$SSIM = \left(\frac{\sigma_{I_1 I_2}}{\sigma_{I_1} \sigma_{I_2}} \right) \left(\frac{2 \bar{I}_1 \bar{I}_2}{(\bar{I}_1^2) + (\bar{I}_2^2)} \right) \left(\frac{2 \sigma_{I_1} \sigma_{I_2}}{(\sigma_{I_1}^2) + (\sigma_{I_2}^2)} \right) \quad (23)$$

The variance of the original image is $\sigma_{I_1}^2$, while the variance of the enhanced image is $\sigma_{I_2}^2$. The SSIM value is calculated for each image. The results of the comparison of 12 images are presented in Table 4.

In this proposed method, SSIM is the fittest value for

optimizing the smoothness factor of BEASF. In Table 4, the SSIM value is higher than the other methods and is approaching 0.99. The proposed method's average SSIM value indicates improved enhancement outcomes of brain tumor MR images [57].

5.2.5 Features Similarity Index Metric (FSIM)

It determines how similar the original and enhanced images are in terms of features. The maximum value of 1 shows a better overall morphology after the contrast enhancement [30]. It is expressed as:

$$FSIM = \frac{\sum_{x \in \mathbb{Y}} S_L(x) PC_m(x)}{\sum_{x \in \mathbb{Y}} PC_m(x)} \quad (24)$$

where, \mathbb{Y} is the whole image spatial domain of the image, $S_L(x)$ is the similarity measures of that phase component and gradient magnitude of the original and enhanced image, and $PC_m(x)$ is the phase component of the original and enhanced image. Table 5 shows the performance of FSIM computed with other state-of-the-art image enhancement methods. From Table 5, the higher values of FSIM of the proposed method show a better-enhanced quality of enhanced MR images. The value of FSIM is about 0.99 for all types of tumor images.

5.2.6 Riesz Transformed based Feature Similarity Index Metric (RFSIM)

It is calculated by comparing the two image feature maps at key points. The Riesz transform coefficient is used as a feature directly. Here I_1 and I_2 are original and enhanced images.

Let $I_{1_1}, I_{1_2}, I_{1_3}, I_{1_4},$ and I_{1_5} are represented as $R_x\{I_1\}, R_y\{I_1\}, R_x\{R_x\{I_1\}\}, R_x\{R_y\{I_1\}\}$ and $R_y\{R_y\{I_1\}\}$. Similarly $I_{2_1}, I_{2_2}, I_{2_3}, I_{2_4}, I_{2_5}$ are represented as $R_x\{I_2\}, R_y\{I_2\}, R_x\{R_x\{I_2\}\}, R_x\{R_y\{I_2\}\}$ and $R_y\{R_y\{I_2\}\}$. Here $R_x\{I_1\}, R_y\{I_1\},$ are first-order coefficient and $R_x\{R_x\{I_2\}\}, R_x\{R_y\{I_2\}\}$ and $R_y\{R_y\{I_2\}\}$ represent the second order coefficient. So the similarity between two features map I_{1_i} and I_{2_i} ($i \sim 5$) at the respective location (x, y) is defined as [58]:

$$d_i(x, y) = \frac{2I_{1_i}(x, y)I_{2_i}(x, y) + C}{I_{1_i}^2(x, y) + I_{2_i}^2(x, y) + C} \quad (25)$$

where, C is a very small constant, the features map's similarity is high, I_{1_i} and I_{2_i} are expressed as:

$$D_i = \frac{\sum \sum d_i(x, y) \times M(x, y)}{\sum \sum M(x, y)} \quad (26)$$

Then, as shown below, we calculate the RFSIM between two images I_1 and I_2 :

$$RFSIM = \prod_{i=1}^5 D_i \quad (27)$$

A higher value of RFSIM, close to 1, shows better enhancement [59]. As per the results shown in Table 6, the value of RFSIM is much better in the proposed method than for the other state-of-the-art methods.

Table 4. Structural similarity index metric value

Method	Glioma Tumor				Meningioma Tumor				Pituitary Tumor			
	901	796	1899	2300	99	500	245	281	1689	1546	1332	1389
CLAHE with Median Filter	0.7311	0.6336	0.7009	0.4215	0.7394	0.7350	0.6678	0.6698	0.6470	0.5699	0.7284	0.7703
CLAHE with Wiener Filter	0.7767	0.6929	0.7525	0.4907	0.7160	0.6993	0.6890	0.7114	0.6501	0.5695	0.7296	0.7535
Decorrelation Stretching	0.8103	0.5136	0.7009	0.6682	0.8826	0.8867	0.7156	0.8831	0.6964	0.8126	0.7228	0.9168
EnhGSA	0.7253	0.8426	0.7244	0.5794	0.6532	0.8034	0.7124	0.7289	0.7399	0.7248	0.7124	0.6890
MMSICHE	0.8545	0.7044	0.7885	0.6448	0.8882	0.8330	0.9064	0.8061	0.7914	0.8731	0.7631	0.8877
VFGLE	0.6774	0.3915	0.4804	0.4044	0.7397	0.7002	0.6838	0.6031	0.5431	0.4316	0.5442	0.1340
BEASF	0.946	0.9153	0.9345	0.9042	0.9568	0.9379	0.9470	0.9642	0.9421	0.9507	0.9474	0.9218
Proposed Method	0.9880	0.9885	0.9838	0.9800	0.9911	0.9841	0.9922	0.9894	0.9876	0.9871	0.9910	0.9907

Table 5. Features similarity index metric value

Method	Glioma Tumor				Meningioma Tumor				Pituitary Tumor			
	901	796	1899	2300	99	500	245	281	1689	1546	1332	1389
CLAHE with Median Filter	0.9836	0.9843	0.9767	0.9168	0.9850	0.9786	0.9673	0.9728	0.9831	0.9534	0.9813	0.9920
CLAHE with Wiener Filter	0.9843	0.9849	0.9683	0.9409	0.9808	0.9773	0.9830	0.9809	0.9816	0.9573	0.9799	0.9912
Decorrelation Stretching	0.9998	0.9994	0.9996	0.9995	0.9998	0.9999	0.9998	0.9999	0.9998	0.9998	0.9994	0.9998
EnhGSA	0.8705	0.9231	0.832	0.8048	0.7775	0.8867	0.8601	0.8317	0.8770	0.8719	0.8492	0.8674
MMSICHE	0.8782	0.7299	0.7767	0.7125	0.9184	0.8415	0.9154	0.8421	0.8263	0.8716	0.7947	0.9269
VFGLE	0.9924	0.9934	0.9871	0.9981	0.9925	0.9939	0.9817	0.9807	0.9919	0.9579	0.9897	0.9956
BEASF	0.9996	0.9995	0.9997	0.9983	0.9998	0.9985	0.9996	0.9997	0.9989	0.9995	0.9995	0.9995
Proposed Method	0.9997	0.9989	0.9993	0.9987	0.9998	0.9992	0.9999	0.9998	0.9997	0.9997	0.9996	0.9999

Table 6. Riesz transformed based feature similarity index metric value

Method	Glioma Tumor				Meningioma Tumor				Pituitary Tumor			
	901	796	1899	2300	99	500	245	281	1689	1546	1332	1389
CLAHE with Median Filter	0.9913	0.9903	0.9907	0.9857	0.9873	0.9858	0.9826	0.9876	0.9836	0.9899	0.9939	0.9921
CLAHE with Wiener Filter	0.9924	0.9917	0.9918	0.9889	0.9851	0.9874	0.9842	0.9866	0.9833	0.9849	0.9937	0.9901
Decorrelation Stretching	0.9760	0.9610	0.9631	0.9594	0.9848	0.9881	0.9580	0.9886	0.9714	0.9696	0.9606	0.9717
EnhGSA	0.2648	0.4330	0.2075	0.0325	0.0925	0.3074	0.2116	0.1718	0.3149	0.1068	0.2074	0.1849
MMSICHE	0.2997	0.0332	0.1066	0.0312	0.3500	0.0991	0.4317	0.1900	0.1052	0.2101	0.1365	0.2922
VFGLE	0.9807	0.9637	0.9723	0.9657	0.9874	0.9797	0.9872	0.9814	0.9727	0.9778	0.9764	0.9918
BEASF	0.9940	0.9933	0.9923	0.9924	0.9957	0.9938	0.9956	0.9968	0.9926	0.9926	0.9957	0.9927
Proposed Method	0.9999	0.9999	0.9999	0.9999	0.9999	0.9999	0.9999	0.9999	0.9999	0.9999	0.9999	0.9999

Table 7. Spectral residual base similarity index metric value

Method	Glioma Tumor				Meningioma Tumor				Pituitary Tumor			
	901	796	1899	2300	99	500	245	281	1689	1546	1332	1389
CLAHE with Median Filter	0.9865	0.9926	0.9927	0.9972	0.9852	0.9782	0.9893	0.9743	0.9857	0.9885	0.9917	0.9860
CLAHE with Wiener Filter	0.9871	0.9923	0.9932	0.9983	0.9864	0.9774	0.9731	0.9683	0.9863	0.9826	0.9938	0.9917
Decorrelation Stretching	0.9993	0.9906	0.9998	0.9960	0.9967	0.9996	0.9998	0.9991	0.9993	0.9997	0.9988	0.9999
EnhGSA	0.9489	0.9660	0.9531	0.9077	0.8447	0.9069	0.9155	0.9139	0.9464	0.9546	0.9441	0.9383
MMSICHE	0.9339	0.8364	0.8844	0.8464	0.9346	0.8698	0.9062	0.8925	0.8509	0.9105	0.8557	0.9426
VFGLE	0.9806	0.9648	0.9610	0.9949	0.9938	0.9755	0.9950	0.9805	0.9950	0.9786	0.9823	0.9932
BEASF	0.9998	0.9976	0.9989	0.9993	0.9947	0.9954	0.9972	0.9995	0.9962	0.9979	0.9974	0.9988
Proposed Method	0.9998	0.9981	0.9998	0.9996	0.9999	0.9996	0.9997	0.9999	0.9998	0.9997	0.9998	0.9999

Table 8. Absolute mean brightness error value

Method	Glioma Tumor				Meningioma Tumor				Pituitary Tumor			
	901	796	1899	2300	99	500	245	281	1689	1546	1332	1389
CLAHE with Median Filter	16.99	35.16	18.95	23.96	30.89	25.66	24.59	21.28	38.59	33.80	24.92	21.36
CLAHE with Wiener Filter	16.49	33.44	17.82	22.74	32.19	25.90	26.94	22.98	39.18	36.37	26.68	23.64
Decorrelation Stretching	9.771	36.11	18.34	10.48	37.97	67.61	31.61	40.66	63.02	31.73	41.57	24.13
EnhGSA	38.13	25.50	38.61	23.17	15.31	35.31	20.06	5.73	43.21	20.34	36.50	50.79
MMSICHE	6.33	7.20	7.71	3.00	10.50	9.75	8.10	8.50	13.17	10.95	14.22	7.42
VFGLE	16.77	59.47	24.24	28.56	38.69	45.22	32.98	35.11	61.47	57.20	59.13	34.16
BEASF	0.422	0.562	0.583	0.122	2.15	3.99	3.55	3.18	5.74	1.37	1.21	8.76
Proposed Method	0.141	0.143	.625	0.255	0.059	0.332	0.195	0.325	7.44	0.350	0.006	0.215

Table 9. Average values of performance evaluation metrics

Performance Evaluation Metrics	Types of Tumors	CLAHE with Median Filter	CLAHE with Wiener Filter	Decorrelation Stretching	EnhGSA	MMSICHE	VFGLE	BEASF	Proposed
MSE	Glioma	0.01535	0.01365	0.02560	1796.54	744.380	0.03817	0.00310	0.00002
	Meningioma	0.01845	0.02432	0.03742	1480.14	568.322	0.03150	0.00222	0.00002
	Pituitary	0.01977	0.02272	0.04138	2376.36	810.498	0.05214	0.00268	0.00002
PSNR	Glioma	18.4500	18.9525	16.3675	16.0400	19.4675	14.9150	25.1625	44.6950
	Meningioma	17.3820	16.1825	14.6200	17.0475	20.6500	15.0900	26.4675	45.2650
	Pituitary	17.3400	16.8000	14.5250	14.3025	19.1100	12.8225	25.5225	45.2525
MAE	Glioma	0.10120	0.09537	0.13030	0.71002	3.79075	0.15527	0.03572	0.00450
	Meningioma	0.11052	0.13007	0.16575	2.01152	1.19815	0.15195	0.04032	0.00435
	Pituitary	0.11852	0.12557	0.16185	0.12390	1.18565	0.20817	0.04322	0.00430
SSIM	Glioma	0.62177	0.67820	0.67325	0.71792	0.74805	0.48842	0.92500	0.98507
	Meningioma	0.70300	0.70392	0.84200	0.72447	0.85842	0.68170	0.95147	0.98920
	Pituitary	0.67890	0.67567	0.78715	0.71652	0.82882	0.41322	0.94050	0.98910
FSIM	Glioma	0.96535	0.96960	0.99957	0.85760	0.77432	0.99275	0.99927	0.99915
	Meningioma	0.97592	0.98050	0.99985	0.83900	0.87935	0.98720	0.99940	0.99967
	Pituitary	0.97745	0.97750	0.99970	0.86637	0.85487	0.98377	0.99935	0.99972
RFSIM	Glioma	0.98950	0.99120	0.96487	0.23445	0.11767	0.97060	0.99300	0.99990
	Meningioma	0.98582	0.98582	0.97987	0.19582	0.26770	0.98392	0.99547	0.99990
	Pituitary	0.98987	0.98800	0.96832	0.20350	0.18600	0.97967	0.99340	0.99990
SRSIM	Glioma	0.99225	0.99272	0.99642	0.94392	0.87527	0.97532	0.99890	0.99932
	Meningioma	0.98175	0.97630	0.99880	0.89525	0.90077	0.98620	0.99670	0.99977
	Pituitary	0.98797	0.98860	0.99942	0.94585	0.88992	0.98727	0.99757	0.99980
AMBE	Glioma	23.7650	22.6225	18.6752	31.3525	6.06000	32.2600	0.42225	0.29100
	Meningioma	25.6050	27.0025	44.4625	19.1025	9.21250	38.0000	3.21750	0.22775
	Pituitary	29.6675	31.4675	40.1125	37.7100	11.4400	52.9900	4.27000	2.00275

Table 10. Friedman's mean rank test value

Method	CLAHE with Median Filter	CLAHE with Wiener Filter	Decorrelation Stretching	EnhGSA	MMSICHE	VFGLE	BEASF	Proposed Method
Friedman's Rank	4.5833	4.4167	4.1667	6.8333	6.7282	5.6111	2.4456	1.1667

5.2.7 Spectral Residual base Similarity Index Metric (SRSIM)

It is based on spectral residual visual saliency mapping approaches. It plays two roles, the first one for characterizing the local quality of an image and the second while assessing the overall quality ratings, demonstrating the relevance of a particular location to the human visual system [60]. SRSIM value range is zero to one. A higher value shows the better quality of the enhanced image. SRSIM between two images is defined as:

$$SRSIM = \frac{\sum_{x \in \Delta} S_L(x) R_m(x)}{\sum_{x \in \Delta} R_m(x)} \quad (28)$$

where, Δ means the entire image special domain, $S_L(x)$ is the similarity, and $R_m(x)$ is the weight importance of $S_L(x)$. SRSIM value is improved in the proposed method and approaches the maximum value that is one. The performance of SRSIM shown in Table 7 strongly recommends the proposed method to enhance brain tumor MR images.

5.2.8 Absolute Mean Brightness Error (AMBE)

It was proposed by Chen et al. in the year 2003 to determine the performance in preserving the originality of an image [61]. It is the difference between the original image and the enhanced image's mean intensity values. It is expressed as:

$$AMBE = |\text{mean intensity of } (I_1) - \text{mean intensity of } (I_2)| \quad (29)$$

The small value of AMBE indicates better enhancement [31]. For the proposed method, values of AMBE are shown in Table 8.

The performance gap with other-state-of-the-art method indicates that better enhancement of brain tumor MR images with the proposed method

The proposed enhancement methodology has been checked on 1577 images in this paper. The results of 12 images (4 of each type) for the evaluation metrics are shown in Tables (1 to 8). An average of each performance evaluation metric has been computed for each tumor type, and the results are indicated in Table 9.

For the proposed method, the minimum value of the MSE average is 0.00002 is much better than BEASF. The worst value is achieved with MMSICHE. The average value of PSNR is around 45, while that of BEASF is 25. MAE is lowest at about 0.004. The average value of SSIM is 0.9877, which is near one means better enhancement. The average value of FSIM is 0.9995, which is higher as compared with other methods. The average value of RFSIM is nearly one (0.9999), and the SRSIM average value is 0.9996. The average value of AMBE is 0.8198 lowest compared with other methods.

5.3 Statistical test

Friedman's mean rank test [62, 63] is used to check the statistical difference between proposed and other state-of-the-art methods. The statistical findings of Friedman's mean rank test for performance evaluation metrics are shown in Table 10. According to the statistical data, the suggested approach is in the first place and surpassed the state-of-the-art methods. The p-value of Friedman's mean rank test is 2.0179×10^{-14} , which is very low compared to $\alpha = 0.05$.

6. CONCLUSIONS

This work has proposed a methodology for enhancing MR images for better diagnosis and treatment of the patients. The enhancement analysis has been made with visual inspection and image quality metrics. A comprehensive learning strategy is used to modify the EHO to get the optimal value of the smoothness factor of the sigmoid function. This optimal value of the sigmoid function gives enhancement of the MR image quality. The proposed methodology tested on brain tumor MR images taken from Figshare. For validation of the method, the value of MSE, PSNR, MAE, SSIM, FSIM, RFSIM, SRSIM, and AMBE have been computed and analyzed. Compared to state-of-the-art approaches, the proposed work has greatly improved the image quality performance metrics. The enhanced image will give better textural, intensity, and shape features used to help accurately detect the brain tumor. The ranking of this method has also been checked using Friedman's mean rank test. The proposed method achieves the first rank, which shows its practical applicability. The enhancement of MR images will improve the detection accuracy of brain tumors and helps in the observation of tumor progress during the treatment.

REFERENCES

- [1] Kirkpatrick, D.B. (1984). The first primary brain-tumor operation. *Journal of Neurosurgery*, 61(5): 809-813. <https://doi.org/10.3171/jns.1984.61.5.0809>
- [2] Rajasekaran, K.A., Gounder, C.C. (2018). Advanced brain tumour segmentation from MRI images. *Basic Physical Principles and Clinical Applications, High-Resolution Neuroimaging*, 83-108. <https://doi.org/10.5772/intechopen.71416>
- [3] Sung, H., Ferlay, J., Siegel, R.L., Laversanne, M., Soerjomataram, I., Jemal, A., Bray, F. (2021). Global cancer statistics 2020: GLOBOCAN estimates of incidence and mortality worldwide for 36 cancers in 185 countries. *CA: A Cancer Journal for Clinician*, 71(3): 209-249. <https://doi.org/10.3322/caac.21660>
- [4] Dasgupta, A., Gupta, T., Jalali, R. (2016). Indian data on central nervous tumors: A summary of published work. *South Asian Journal of Cancer*, 5(3): 147-153. <https://doi.org/10.4103/2278-330X.187589>
- [5] Cokkinides, V., Albano, J., Samuels, A., Ward, M., Thum, J. (2005). *American cancer society: Cancer facts and figures*. Atlanta: American Cancer Society.
- [6] Zacharaki, E.L., Wang, S., Chawla, S., Soo Yoo, D., Wolf, R., Melhem, E.R., Davatzikos, C. (2009). Classification of brain tumor type and grade using MRI texture and shape in a machine learning scheme. *Magnetic Resonance in Medicine: An Official Journal of the International Society for Magnetic Resonance in Medicine*, 62(6): 1609-1618. <https://doi.org/10.1002/mrm.22147>
- [7] Abdallah, Y.M.Y. (2017). History of medical imaging. *Archives of Medicine and Health Sciences*, 5(2): 275-281. https://doi.org/10.4103/amhs.amhs_97_17
- [8] Choksey, M.S., Valentine, A., Shawdon, H., Freer, C.E., Lindsay, K.W. (1989). Computed tomography in the diagnosis of malignant brain tumours: Do all patients require biopsy? *Journal of Neurology, Neurosurgery & Psychiatry*, 52(7): 821-825.

- <https://doi.org/10.1136/jnnp.52.7.821>
- [9] Seetha, J., Raja, S.S. (2018). Brain tumor classification using convolutional neural networks. *Biomedical & Pharmacology Journal*, 11(3): 1457-1461. <https://doi.org/10.13005/bpj/1511>
- [10] Wood, M.L., Runge, V.M. (1988). Application of image enhancement techniques to magnetic resonance imaging. *Radiographics*, 8(4): 771-784. <https://doi.org/10.1148/radiographics.8.4.3051162>
- [11] Xue, J.H., Philips, W., Pizurica, A., Lemahieu, I. (2001). A novel method for adaptive enhancement and unsupervised segmentation of MRI brain image. In 2001 IEEE International Conference on Acoustics, Speech, and Signal Processing. Proceedings (Cat. No. 01CH37221), Lake City, UT, USA, pp. 2013-2016. <https://doi.org/10.1109/ICASSP.2001.941344>
- [12] Christensen, J.D. (2003). Normalization of brain magnetic resonance images using histogram even-order derivative analysis. *Magnetic Resonance Imaging*, 21(7): 817-820. [https://doi.org/10.1016/S0730-725X\(03\)00102-4](https://doi.org/10.1016/S0730-725X(03)00102-4)
- [13] Weisenfeld, N.L., Warfield, S.K. (2004). Normalization of joint image-intensity statistics in MRI using the Kullback-Leibler divergence. In 2004 2nd IEEE International Symposium on Biomedical Imaging: Nano to Macro (IEEE Cat No. 04EX821), Arlington, VA, USA, pp. 101-104. <https://doi.org/10.1109/isbi.2004.1398484>
- [14] Joshi, S.H., Marquina, A., Osher, S.J., Dinov, I., Van Horn, J.D., Toga, A.W. (2009). MRI resolution enhancement using total variation regularization. In 2009 IEEE International Symposium on Biomedical Imaging: From Nano to Macro, Boston, MA, USA, pp. 161-164. <https://doi.org/10.1109/ISBI.2009.5193008>
- [15] Liu, X.S., Nie, S.D., Sun, X.W. (2009). An enhancement method for small brain metastases in T1w MRI. In 2009 Sixth International Conference on Fuzzy Systems and Knowledge Discovery, Tianjin, China, pp. 416-419. <https://doi.org/10.1109/FSKD.2009.256>
- [16] Rajeesh, J., Moni, R.S., Palanikumar, S., Gopalakrishnan, T. (2010). Noise reduction in magnetic resonance images using wave atom shrinkage. *International Journal of Image Processing (IJIP)*, 4(2): 131-141.
- [17] Khademi, A., Venetsanopoulos, A., Moody, A.R. (2010). Image enhancement and noise suppression for FLAIR MRIs with white matter lesions. *IEEE Signal Processing Letters*, 17(12): 989-992. <https://doi.org/10.1109/LSP.2010.2082527>
- [18] Rallabandi, V.S., Roy, P.K. (2010). Magnetic resonance image enhancement using stochastic resonance in Fourier domain. *Magnetic Resonance Imaging*, 28(9): 1361-1373. <https://doi.org/10.1016/j.mri.2010.06.014>
- [19] Bandyopadhyay, S.K. (2011). Image enhancement technique applied to low-field MR brain images. *International Journal of Computer Applications*, 975: 8887. <https://doi.org/10.5120/1956-2617>
- [20] George, E.B., Karnan, M. (2012). MRI Brain Image enhancement using filtering techniques. *International Journal of Computer Science & Engineering Technology*, 3(9): 399-403.
- [21] Birla, A., Shantaiya, S. (2015). Performance analysis of image enhancement techniques for brain tumor images. *International Journal of Emerging Trends & Technology in Computer Science*, 2(8): 94-97.
- [22] Sharma, Y., Meghrajani, Y.K. (2014). Extraction of grayscale brain tumor in magnetic resonance image. *International Journal of Advanced Research in Computer and Communication Engineering*, 3(11): 8542-8545. <https://doi.org/10.17148/ijarccce.2014.31142>
- [23] Benson, C.C., Lajish, V.L. (2014). Morphology based enhancement and skull stripping of MRI brain images. In 2014 International Conference on Intelligent Computing Applications, Coimbatore, India, pp. 254-257. <https://doi.org/10.1109/ICICA.2014.61>
- [24] Chen, C.M., Chen, C.C., Wu, M.C., Horng, G., Wu, H.C., Hsueh, S.H., Ho, H.Y. (2015). Automatic contrast enhancement of brain MR images using hierarchical correlation histogram analysis. *Journal of Medical and Biological Engineering*, 35(6): 724-734. <https://doi.org/10.1007/s40846-015-0096-6>
- [25] Natteshan, N.V.S., Angel Arul Jothi, J. (2015). Automatic classification of brain MRI images using SVM and neural network classifiers. *Advances in Intelligent Informatics*, pp. 19-30. https://doi.org/10.1007/978-3-319-11218-3_3
- [26] Deng, H., Deng, W., Sun, X., Ye, C., Zhou, X. (2016). Adaptive intuitionistic fuzzy enhancement of brain tumor MR images. *Scientific Reports*, 6(1): 25760. <https://doi.org/10.1038/srep35760>
- [27] Kaur, H., Rani, J. (2016). MRI brain image enhancement using Histogram equalization Techniques. In 2016 International Conference on Wireless Communications, Signal Processing and Networking (WiSPNET), Chennai, India, pp. 770-773. <https://doi.org/10.1109/WiSPNET.2016.7566237>
- [28] Viswanath, K. (2017). Enhancement of brain tumor images. In 2017 2nd IEEE International Conference on Recent Trends in Electronics, Information & Communication Technology (RTEICT), Bangalore, India, pp. 1894-1898. <https://doi.org/10.1109/RTEICT.2017.8256926>
- [29] Min, A., Kyu, Z.M. (2017). MRI images enhancement and tumor segmentation for brain. In 2017 18th International Conference on Parallel and Distributed Computing, Applications and Technologies (PDCAT), Taipei, Taiwan, pp. 270-275. <https://doi.org/10.1109/PDCAT.2017.00051>
- [30] Subramani, B., Veluchamy, M. (2018). MRI brain image enhancement using brightness preserving adaptive fuzzy histogram equalization. *International Journal of Imaging Systems and Technology*, 28(3): 217-222. <https://doi.org/10.1002/ima.22272>
- [31] Mzoughi, H., Njeh, I., Slima, M.B., Hamida, A.B. (2018). Histogram equalization-based techniques for contrast enhancement of MRI brain Glioma tumor images: Comparative study. In 2018 4th International conference on advanced technologies for signal and image processing (ATSIP), Sousse, Tunisia, pp. 1-6. <https://doi.org/10.1109/ATSIP.2018.8364471>
- [32] Singh, L.S., Ahlawat, A.K., Singh, K.M., Singh, T.R., Singh, Y.S. (2019). Medical image enhancement using fuzzy and regression based neural network approach. *International Journal of Applied Engineering Research*, 14(7): 1532-1538.
- [33] Bhateja, V., Nigam, M., Bhadauria, A.S., Arya, A., Zhang, E.Y.D. (2019). Human visual system based optimized mathematical morphology approach for enhancement of brain MR images. *Journal of Ambient Intelligence and Humanized Computing*.

- <https://doi.org/10.1007/s12652-019-01386-z>
- [34] Acharya, U.K., Kumar, S. (2020). Particle swarm optimized texture based histogram equalization (PSOTHE) for MRI brain image enhancement. *Optik*, 224: 165760. <https://doi.org/10.1016/j.ijleo.2020.165760>
- [35] Vidyasaraswathi, H.N., Hanumantharaju, M.C. (2020). Brain MR image enhancement using average intensity replacement based on GWOHE algorithm. *International Journal of Engineering and Advanced Technology*, 9(3): 3193-3199. <https://doi.org/10.35940/ijeat.c6072.029320>
- [36] Ullah, Z., Lee, S.H., An, D. (2020). Histogram equalization based enhancement and MR brain image skull stripping using mathematical morphology. *International Journal of Advanced Computer Science and Applications*, 11(3): 569-577. <https://doi.org/10.14569/IJACSA.2020.0110372>
- [37] Sabitha, R., Shanthini, J., Kavitha, M.S., Bhavadharini, R.M., Chellaprabha, B. (2021). Contrast enhancement for MRI image using hybrid optimization technique. *Annals of the Romanian Society for Cell Biology*, 25(2): 2554-2566.
- [38] Sreenivasulu, N., Ravi Kishore, M. (2015). Color image enhancement using adaptive sigmoid function with bi-Histogram equalization. *International Journal of Engineering Research & Technology*, 3(12): 1-7.
- [39] Sandeep, Suresha, M. (2019). Enhancement of low-quality images using Bi-Histogram equalization adaptive sigmoid function based on shifted Gompertz distribution. *International Journal of Computer Sciences and Engineering*, 7(1): 185-191. <https://doi.org/10.26438/ijcse/v7i1.185191>
- [40] Arriaga-Garcia, E.F., Sanchez-Yanez, R.E., Garcia-Hernandez, M.G. (2014). Image enhancement using Bi-Histogram equalization with adaptive sigmoid functions. In 2014 International Conference on Electronics, Communications and Computers (CONIELECOMP), Cholula, Mexico, pp. 28-34. <https://doi.org/10.1109/CONIELECOMP.2014.6808563>
- [41] Wang, G.G., Deb, S., Coelho, L.D.S. (2015). Elephant herding optimization. In 2015 3rd International Symposium on Computational and Business Intelligence (ISCBI), Bali, Indonesia, pp. 1-5. <https://doi.org/10.1109/ISCBI.2015.8>
- [42] Ismaeel, A.A., Elshaarawy, I.A., Houssein, E.H., Ismail, F.H., Hassanien, A.E. (2019). Enhanced elephant herding optimization for global optimization. *IEEE Access*, 7: 34738-34752. <https://doi.org/10.1109/ACCESS.2019.2904679>
- [43] Singh, H., Singh, B., Kaur, M. (2021). An improved elephant herding optimization for global optimization problems. *Engineering with Computers*. <https://doi.org/10.1007/s00366-021-01471-y>
- [44] Zhang, Y., Jin, Z. (2021). Comprehensive learning Jaya algorithm for engineering design optimization problems. *Journal of Intelligent Manufacturing*, 33: 1229-1253. <https://doi.org/10.1007/s10845-020-01723-6>
- [45] Cheng, J., Huang, W., Cao, S., et al. (2015). Correction: enhanced performance of brain tumor classification via tumor region augmentation and partition. *PloS One*, 10(12): e0144479. <https://doi.org/10.1371/journal.pone.0140381>
- [46] Beohar, R., Sahu, P. (2013). Performance analysis of underwater image enhancement with CLAHE 2D median filtering technique on the basis of SNR, RMS error, mean brightness. *International Journal of Engineering and Innovative Technology*, 3(2): 525-528.
- [47] Kalfon, M., Porat, M. (2013). A new approach to texture recognition using decorrelation stretching. *International Journal of Future Computer and Communication*, 2(1): 49-53. <https://doi.org/10.7763/IJFCC.2013.V2.119>
- [48] Katircioğlu, F., Cingiz, Z. (2020). A novel gray image enhancement using the regional similarity transformation function and dragonfly algorithm. *El-Cezeri Journal of Science and Engineering*, 7(3): 1201-1219. <https://doi.org/10.31202/ecjse.733519>
- [49] Singh, K., Kapoor, R. (2014). Image enhancement via median-mean based sub-image-clipped histogram equalization. *Optik*, 125(17): 4646-4651. <https://doi.org/10.1016/j.ijleo.2014.04.093>
- [50] Tian, Q.C., Cohen, L.D. (2018). A variational-based fusion model for non-uniform illumination image enhancement via contrast optimization and color correction. *Signal Processing*, 153: 210-220. <https://doi.org/10.1016/j.sigpro.2018.07.022>
- [51] Sharma, P., Sharma, S., Goyal, A. (2016). An MSE (mean square error) based analysis of deconvolution techniques used for deblurring/restoration of MRI and CT Images. In Proceedings of the Second International Conference on Information and Communication Technology for Competitive Strategies, Udaipur, India, 51. <https://doi.org/10.1145/2905055.2905257>
- [52] Wu, Q., Fan, J., Wu, F., Zhao, J., Qian, L. (2013). Error analysis of the Golay3 optical imaging system. *Applied Optics*, 52(13): 2966-2973. <https://doi.org/10.1364/AO.52.002966>
- [53] Veluchamy, M., Mayathevar, K., Subramani, B. (2019). Brightness preserving optimized weighted Bi-Histogram equalization algorithm and its application to MR brain image segmentation. *International Journal of Imaging Systems and Technology*, 29(3): 339-352. <https://doi.org/10.1002/ima.22330>
- [54] Wang, Z., Bovik, A.C., Sheikh, H.R., Simoncelli, E.P. (2004). Image quality assessment: From error visibility to structural similarity. *IEEE Transactions on Image Processing*, 13(4): 600-612. <https://doi.org/10.1109/TIP.2003.819861>
- [55] Kiran, B.K. (2019). Implementation of tumor prediction system using classification algorithms. *International Journal of Engineering and Advanced Technology*, 9(2): 4507-4511. <https://doi.org/10.35940/ijeat.B4664.129219>
- [56] Zujovic, J., Pappas, T.N., Neuhoff, D.L. (2013). Structural texture similarity metrics for image analysis and retrieval. *IEEE Transactions on Image Processing*, 22(7): 2545-2558. <https://doi.org/10.1109/TIP.2013.2251645>
- [57] Katouli, M., Rahmani, A.E. (2020). Brain tumor diagnosis in MRI images using image processing techniques and pixel-based clustering. *Treatment du Signal*, 37(2): 291-300. <https://doi.org/10.18280/ts.370215>
- [58] Zhang, L., Zhang, L., Mou, X. (2010). RFSIM: A feature based image quality assessment metric using Riesz transforms. In 2010 IEEE International Conference on Image Processing, Hong Kong, China, pp. 321-324. <https://doi.org/10.1109/ICIP.2010.5649275>
- [59] Zada, S., Darfi, S., Dembele, V., Rachafi, S., Nassim, A. (2013). Temperature measurement method based on

- Riesz transform method. *International Scholarly Research Notices*, 2013: 967357.
<https://doi.org/10.1155/2013/967357>
- [60] Zhang, L., Li, H. (2012). SR-SIM: A fast and high performance IQA index based on spectral residual. In 2012 19th IEEE International Conference on Image Processing, Orlando, FL, USA, pp. 1473-1476.
<https://doi.org/10.1109/ICIP.2012.6467149>
- [61] Chen, S.D., Ramli, A.R. (2003). Minimum mean brightness error Bi-Histogram equalization in contrast enhancement. *IEEE Transactions on Consumer Electronics*, 49(4): 1310-1319.
<https://doi.org/10.1109/TCE.2003.1261234>
- [62] Friedman, M. (1937). The use of ranks to avoid the assumption of normality implicit in the analysis of variance. *Journal of the American Statistical Association*, 32(200): 675-701.
<https://doi.org/10.1080/01621459.1937.10503522>
- [63] Friedman, M. (1940). A comparison of alternative tests of significance for the problem of SMS rankings. *The Annals of Mathematical Statistics*, 11(1): 86-92.
<https://doi.org/10.1214/aoms/1177731944>